Modeled Contrast in the Response of the Surface Energy Balance to Heat Waves for Forest and Grassland

LENNERT B. STAP AND BART J. J. M. VAN DEN HURK

Institute for Marine and Atmospheric Research Utrecht, Utrecht University, Utrecht, and Royal Netherlands Meteorological Institute (KNMI), De Bilt, Netherlands

CHIEL C. VAN HEERWAARDEN

Max Planck Institute for Meteorology, Hamburg, Germany

ROEL A. J. NEGGERS

Royal Netherlands Meteorological Institute (KNMI), De Bilt, Netherlands

(Manuscript received 14 February 2013, in final form 20 November 2013)

ABSTRACT

Observations have shown that differences in surface energy fluxes over grasslands and forests are amplified during heat waves. The role of land–atmosphere feedbacks in this process is still uncertain. In this study, a single-column model (SCM) is used to investigate the difference between forest and grassland in their energy response to heat waves. Three simulations for the period 2005–11 were carried out: a control run using vegetation characteristics for Cabauw (the Netherlands), a run where the vegetation is changed to 100% forest, and a run with 100% short grass as vegetation. A surface evaporation tendency equation is used to analyze the impact of the land–atmosphere feedbacks on evapotranspiration and sensible heat release under normal summer and heat wave conditions with excessive shortwave radiation.

Land–atmosphere feedbacks modify the contrast in surface energy fluxes between forest and grass, particularly during heat wave conditions. The surface resistance feedback has the largest positive impact, while boundary layer feedbacks generally tend to reduce the contrast. Overall, forests give higher air temperatures and drier atmospheres during heat waves. In offline land surface model simulations, the difference between forest and grassland during heat waves cannot be diagnosed adequately owing to the absence of boundary layer feedbacks.

1. Introduction

A recent number of major heat wave and drought events in Europe, the United States, and Russia have triggered considerable research aimed at understanding the underlying mechanisms, trends, socioeconomic effects, predictability, and future projections (e.g., Zaitchik et al. 2006; Ciais et al. 2005; Fischer et al. 2007; Dole et al. 2011; Sheffield et al. 2012). A relationship between temperature extremes and land surface conditions is explored in various studies. Teuling et al. (2010) analyzed the contrast in the surface energy balance response to heat waves between forest and grassland surface types from tower observations and found a systematic difference in partitioning of the anomalous radiation energy over sensible and latent heat. While grasslands tend to use the excess received radiative energy during heat waves mostly for evapotranspiration–latent heat release, forests preserve soil water and use the energy mostly for sensible heat release. The resulting higher atmospheric temperatures over forests enhance the heat wave intensity. If the heat wave continues long enough, this is followed by a reversed contrast when the grassland evaporation leads to soil water depletion. Observations analyzed by Hirschi et al. (2011) clearly indicate the role of antecedent precipitation anomalies (a proxy for variability in soil moisture), where high initial soil moisture values significantly reduce the probability for excessively high temperatures. Pitman et al. (2012) make a link between land use change and trends in both mean

Corresponding author address: Bart van den Hurk, KNMI, P.O. Box 201, 3730 AE De Bilt, Netherlands.
E-mail: hurkvd@knmi.nl

DOI: 10.1175/JHM-D-13-029.1

and extreme temperature worldwide, showing a significant decrease in the number of very hot days in areas with widespread conversions from natural vegetation to crops and pasture in many climate model simulations. The lack of agreement between models and the rather diverse approaches to represent land–atmosphere interactions in these models call for further analysis.

Land–atmosphere interactions play an important role in the response of the surface energy balance to excessive temperatures (Seneviratne et al. 2010). Surface flux anomalies lead to adjustment of the profiles of the overlying atmosphere, which can provide a positive or negative feedback to the strength of the surface fluxes. Apart from a change of the atmospheric properties in direct response to the surface energy balance, an adjustment of the boundary layer dynamics may lead to a change of the near-surface atmospheric properties via entrainment processes (van Heerwaarden et al. 2009), cloud processes (Ek and Holtslag 2004), or the triggering of convection (Findell et al. 2011; Taylor et al. 2012).

The contrasting forest–grassland response as found by Teuling et al. (2010) is relevant for many applications where land use or land use change play a role: adaptation to extreme climate impacts, evaluation of climate effects of reforestation–deforestation, assessing trends in extremes, etc. For many of these applications, numerical models are used as a tool. A verification of the findings in state-of-the-art modeling tools is therefore of great interest.

However, an evaluation using offline land model experiments, as frequently applied in the area of land surface modeling (van den Hurk et al. 2011), has its limitations, as it cannot reproduce these land–atmosphere feedbacks adequately. Van Heerwaarden et al. (2010) developed a conceptual land surface–boundary layer model framework and explored the significance of land–atmosphere feedbacks for two contrasting sites in the Netherlands and the Sahel. In this conceptualization, the land surface and boundary layer processes were represented with a relatively low level of complexity, and the effects of clouds, convection, or other processes affecting the vertical structure of the boundary layer were not included.

In this study, we explore the role of land–atmosphere interaction in creating a contrasting response to heat waves for forest and grassland surface types in a state-of-the-art single-column version of the EC-Earth model (Hazeleger et al. 2012) and the Regional Atmospheric Climate Model, version 2 (RACMO2; van Meijgaard et al. 2008). The model is used to reconstruct meteorological and land surface conditions representative for the Cabauw observational site (van Ulden and Wieringa 1996) for a 7-yr period. Cabauw has a mild climate and does not experience severe drought very often. Different simulations are applied using different surface conditions (grass, forest, and the actual vegetation of Cabauw). The contrasting evaporation response during heat wave conditions is separated into direct responses and feedbacks using the framework developed by van Heerwaarden et al. (2010). Of particular interest is the degree to which feedbacks affect the difference in evapotranspiration response between grassland and forest during heat waves.

Also, we investigated the sensitivity to the individual components that differ between grassland and forest in the model. We did three simulations, changing only one component to the forest value and leaving the rest of the settings to grassland settings.

Parallel to the single-column simulations, offline land scheme simulations are performed. A comparison with the coupled simulations allows a quantification of the land–atmosphere feedback strength. Land–atmosphere feedbacks are expected to lead to different heat wave flux anomalies for forests and grassland. The absence of these feedbacks in the offline runs presumably leads to a different forest–grassland response contrast.

The next section will describe the feedback analysis methodology, the modeling framework, and the experimental setup used in this study in more detail. In section 3, an evaluation of model results using observations is presented, followed by a description of the diurnal cycle of evaporation and its forcings and feedbacks during typical heat wave and non–heat wave conditions. Subsequently, a climatology of the relevant forcing and feedback terms is presented and discussed. This will be compared to simulations with offline land models that do not include these feedbacks and some general conclusions will be drawn from this.

2. Methods and models

a. *The feedback analysis framework*

Van Heerwaarden et al. (2010) used a mixed layer boundary layer model (Tennekes 1973) in combination with the Penman–Monteith equation for surface evaporation:

$$\mathrm{LE} = \frac{\Delta(R_{\mathrm{net}} - G) + \dfrac{\rho c_p}{r_a}(q_{\mathrm{sat}} - q)}{\Delta + \dfrac{c_p}{L}\left(1 + \dfrac{r_a}{r_s}\right)}, \tag{1}$$

where L is the latent heat for vaporization, E is the water vapor flux, Δ is the slope of the saturation specific humidity (q_{sat}) with temperature, R_{net} is the net radiation,

G the soil heat flux, ρ is the air density, c_p the specific heat of dry air, $q_{\text{sat}} - q$ is the water vapor deficit (where q is the actual specific humidity), r_a is the aerodynamic resistance, and r_s is the surface resistance. The boundary layer model gives expressions for the boundary layer height h, the well-mixed boundary layer potential temperature θ and specific humidity q, and a temperature and moisture jump at the top of the boundary layer [($\Delta\theta$ and Δq), here Δ means change] as a function of the sensible heat flux H and the lapse rates of temperature and specific humidity (γ_θ and γ_q) above the boundary layer. With this model framework, they evaluated the diurnal cycle of surface evaporation for two locations (Cabauw in the Netherlands and Niamey in Niger). An analytical solution of the time derivative of evaporation ($\partial\text{LE}/\partial t$) was developed, where dependencies on (external) forcings (radiation, advection) and feedbacks could be distinguished:

$$\frac{\partial \text{LE}}{\partial t} = \begin{cases} c_0\Delta\left[(1-\alpha)\dfrac{\partial S_{\text{in}}}{\partial t} + \dfrac{\partial L_{\text{in}}}{\partial t}\right] \\ +c_0\left(H\Delta^2 + \dfrac{\rho c_p}{r_a}\Delta\right)\text{adv}_\theta - c_0\dfrac{\rho c_p}{r_a}\text{adv}_q \\ +c_0\left(H\Delta^2 + \dfrac{\rho c_p}{r_a}\Delta\right)\left(\dfrac{H}{\rho c_p h} + \dfrac{w_e\Delta\theta}{h}\right) - c_0\dfrac{\rho c_p}{r_a}\left(\dfrac{\text{LE}}{\rho L h} + \dfrac{w_e\Delta q}{h}\right), \\ -c_0\left[\dfrac{\rho c_p}{r_a^2}(q_{\text{sat}} - q) - \text{LE}\dfrac{c_p}{L}\dfrac{r_s}{r_a^2}\right]\dfrac{\partial r_a}{\partial t} \\ -c_0\left(\Delta\dfrac{\partial L_{\text{out}}}{\partial t} + \Delta\dfrac{\partial G}{\partial t} + \dfrac{\text{LE}c_p}{L r_a}\dfrac{\partial r_s}{\partial t}\right) \end{cases} \tag{2}$$

where

$$c_0 = \frac{1}{\Delta + \dfrac{c_p}{L}\left(1 + \dfrac{r_s}{r_a}\right)} \tag{3}$$

is a gain factor. The symbols not yet described above will be explained in the following descriptions of the various components of this equation.

1) Surface radiation forcings

The top row in Eq. (2) describes the tendencies of the radiative forcings on the evaporation: downward shortwave radiation S_{in} (modulated by surface albedo α) and downward longwave radiation L_{in}. Both terms are positively related to the evaporation tendency, since more radiation leads to more evapotranspiration.

2) Boundary layer forcings

The second row shows the effect of boundary layer advection of heat (adv_θ) and moisture (adv_q) on LE. Heat advection enhances evapotranspiration through an increase in specific humidity deficit $q_{\text{sat}} - q$, while advected moisture acts negatively on evapotranspiration by decreasing the ability of the atmosphere to take up moisture.

3) Boundary layer feedbacks

The third row in Eq. (2) shows a number of feedbacks between the surface evaporation and the dynamics and state of the boundary layer. Four terms are distinguished.

i) In the surface warming feedback (term involving $H/\rho c_p h$), surface sensible heat H warms the atmosphere, which will increase its ability to take up moisture. This will lead to more evapotranspiration and constrain the amount of energy available for sensible heat release:

$$H\uparrow \rightarrow \theta\uparrow \rightarrow \text{LE}\uparrow \rightarrow H\downarrow .$$

ii) The entrainment warming feedback (term involving $w_e\Delta\theta/h$) represents entrainment of warm air at the top of the boundary layer (governed by boundary layer growth rate w_e and inversion strength $\Delta\theta$) that also warms the boundary layer and thereby increases its water demand. This leads to increased evapotranspiration, which eventually reduces boundary layer growth:

$$h\uparrow \rightarrow \theta\uparrow \rightarrow \text{LE}\uparrow \rightarrow H\downarrow \rightarrow h\downarrow .$$

iii) In the surface evaporation feedback (term involving $\text{LE}/\rho L h$) evapotranspiration will increase the amount

of moisture in the atmosphere, leading to a negative evaporation feedback:

$$\mathrm{LE}\uparrow \rightarrow q\uparrow \rightarrow \mathrm{LE}\downarrow .$$

iv) The entrainment drying feedback (term involving $w_e\Delta q/h$) represents entrainment of dry air at the top of the boundary layer, thereby increasing evapotranspiration. This will reduce sensible heat release and, consequently, boundary layer growth:

$$q\downarrow \rightarrow \mathrm{LE}\uparrow \rightarrow H\downarrow \rightarrow h\downarrow \rightarrow q\uparrow .$$

The temperature-related processes act positively on evapotranspiration, while moistening of the atmosphere reduces evapotranspiration. All feedback loops are negative, pushing back the perturbed variable toward its original state.

4) Surface layer feedback

The fourth row in Eq. (2) represents the surface layer feedback. If the aerodynamic resistance increases, sensible heat release is constrained. This leads to an increased temperature gradient between the surface and the atmosphere, reducing the atmospheric stability and finally leading to a lower aerodynamic resistance. The significance of this term is dependent on the relative strength of r_a in the overall surface exchange process, which is sensitive to the value of the aerodynamic roughness length (Jacobs and De Bruin 1992). However, van Heerwaarden et al. (2010) demonstrate that this feedback is relatively weak, except during the transitional hours where the sign of the sensible heat flux changes sign. The aerodynamic resistance does affect the gradient of moisture and heat, and this may impose on effects of the other feedbacks in which surface temperature and moisture play a role (land surface feedbacks; see below).

5) Land surface feedbacks

The final row in Eq. (2) depicts three land surface processes that play a role in the daily cycle of evapotranspiration. Outgoing longwave radiation (first term) and ground heat flux (second term) affect the surface temperature and will limit the amount of energy available for latent heat release. An increase in surface resistance r_s (third term), related to smaller stomatal conductance due to, for instance, lower radiation levels, soil drying, or an increase of $q_{\mathrm{sat}} - q$, leads to lower evapotranspiration rates. A reduction of the soil moisture depletion and a lower supply of moisture to the atmosphere will reduce the evaporative stress and thus lead to a lower surface resistance.

We will now describe the structure of the single-column model used in this study, followed by a discussion of retrieving the proper diagnostics from this model output used to evaluate the evaporative forcings and feedbacks depicted by Eq. (2).

b. *The single-column model and the land surface representation*

The single-column model (SCM) used in this study is based on the physical parameterization of the European Centre for Medium-Range Weather Forecasting (ECMWF). It is the standard package in EC-Earth (Hazeleger et al. 2012) and RACMO2 (van Meijgaard et al. 2008). It consists of a series of parameterization schemes discretized on a vertical grid with 91 levels where the atmospheric state variables such as temperature, humidity, and wind speed are calculated. At each level, lateral tendencies of these variables are supplied from daily RACMO2 forecasts initialized and forced by ECMWF reanalysis data. The model is incorporated in a software environment designed for systematic SCM evaluation [the Royal Netherlands Meteorological Institute (KNMI) test bed; Neggers et al. 2012].

The parameterization schemes for cloud physics and boundary layer transport are described in detail by Neggers et al. (2009) and Neggers (2009). The remainder of the subgrid physics of the SCM (land surface, radiation, and convection) is identical to that of cycle 31r1 of the ECMWF Integrated Forecasting System (see www.ecmwf.int/research/ifsdocs/).

The Tiled ECMWF Scheme for Surface Exchanges over Land (TESSEL; van den Hurk 2000) is used in the SCM. It solves the surface energy balance for six subgrid land fractions (high vegetation, low vegetation, bare soil, snow on bare soil–low vegetation, snow under high vegetation, and interception reservoir). Weighted average fluxes are used as a lower boundary condition for the atmospheric model. For high and low vegetation, it uses vegetation-type specific parameters for surface resistance, rooting depth, leaf area index, and aerodynamic roughness from a database within a total of 20 different surface and vegetation types. Evapotranspiration comes from four sources: vegetation, bare soil, the interception layer, and snow sublimation. Under the land surface, a single soil column with four layers of depths 7, 21, 72, and 189 cm (2.89 m in total) is included, where soil water and soil temperature evolve using prognostic equations including thermal and moisture diffusion, gravity drainage, root extraction, and soil freezing. The root zone distribution of TESSEL, listed in Table 1, is described by Zeng et al. (1998). It is based on a comprehensive global

TABLE 1. Surface properties of forest and grassland in TESSEL (van den Hurk et al. 2000).

Variable	Description	Forest	Grassland
LAI	Leaf area index ($m^2\,m^{-2}$)	5	2
$r_{s,\min}$	Minimum stomatal resistance ($s\,m^{-1}$)	500	110
g_d	Parameter in vapor pressure deficit stress function for r_s (mb^{-1})	0.03	0
R_1	Fraction of roots in soil layer 1 of 7-cm depth (%)	26	35
R_2	Fraction of roots in soil layer 2 of 21-cm depth (%)	39	38
R_3	Fraction of roots in soil layer 3 of 72-cm depth (%)	29	23
R_4	Fraction of roots in soil layer 4 of 189-cm depth (%)	6	4
Λ_{sk}	Thermal conductivity of skin layer ($W\,m^{-2}\,K$)	20	10
w_{pwp}	Soil moisture content at wilting point ($m^3\,m^{-3}$)	0.171	0.171
W_{fc}	Soil moisture content at field capacity ($m^3\,m^{-3}$)	0.323	0.323
α	Surface snow-free albedo (–)	0.16	0.20
z_0	Surface roughness length for momentum (m)	2.0	0.02
z_{0h}	Surface roughness length for heat (m)	2.0	0.002

TABLE 2. Characteristics for the different SCM simulations Cabauw, forest, and grassland.

Property	Cabauw	Forest	Grassland
Gridbox fraction high vegetation (%)	1.5	100	0
Gridbox fraction low vegetation (%)	79.5	0	100
Gridbox fraction bare ground (%)	19.0	0	0
Roughness length for momentum (m)	0.25	2.0	0.02
Roughness length for heat (m)	0.0004	2.0	0.002
Surface albedo	0.186	0.16	0.20

root database, and its effect on evapotranspiration and soil wetness is validated by measurements on several locations, including Cabauw.

Of particular interest for the present study is the treatment of surface evaporation by the different vegetation types. Surface evaporation is governed by a so-called Jarvis–Stewart surface resistance formulation that includes multiplicative stress functions sensitive to incoming shortwave radiation, soil moisture, and atmospheric moisture deficit. The latter stress function is only applied to high vegetation (forest) surface types, to express an extra evaporative control such as the response found by Teuling et al. (2010). Table 1 summarizes the differences between grassland and forest as explored in the present study. The values are default implementations of the ECMWF model configuration. Different land surface models obviously carry different parameterizations of all of their components, but a land surface model comparison is not the primary scope of this study. Alternative values of the parameters listed in Table 1 are thus not evaluated here.

c. Simulation setup

The SCM is configured for Cabauw, the Netherlands (51.971°N, 4.927°E, 0.7 m below sea level). The surrounding area is dominated by agricultural activities, and variations in surface height are small (van Ulden and Wieringa 1996). Site observations are stored in the Cabauw Experimental Site for Atmospheric Research (CESAR) database (www.cesar-database.nl). The site was also analyzed by Teuling et al. (2010) and compared to the nearby forest site Loobos. Here we will make simulations with specified settings for Cabauw and simulations in which the surface vegetation specifications were set to evergreen needleleaf forest or short grassland coverage (van den Hurk et al. 2000), with parameter settings as listed in Table 1 (see Table 2 for a simulation overview).

Also, we did three sensitivity runs, using grassland settings with only one component (g_d, $r_{s,\min}$/LAI, and the root fractions in the different soil layers) changed to its forest value.

The run with settings representing the actual Cabauw situation is used as a reference run for evaluation purposes only, set up to closely match observations. Therefore, in the reference Cabauw run, the soil moisture is reinitialized daily to keep the SCM aligned with the driving meteorological conditions provided by RACMO2. For each run, soil moisture is treated as a transient prognostic quantity. This ensures that soil moisture is a property of the specific vegetation type of the run. This differs from the setup of multiple vegetation types coexisting in a single grid point, who share a single soil water reservoir. Also, for the reference Cabauw run, the surface roughness and surface albedo are specified consistent with RACMO2, while vegetation-specific values are used in the other simulations (see Table 2).

The setup of the SCM simulations as adopted here is described in detail by Neggers et al. (2012). Daily SCM simulations are executed between 1 January 2005 and 31 December 2011, in which three heat waves were recorded in the Netherlands: 18–24 June 2005 (7 days), 30 June to 6 July 2006 (7 days), and 15–30 July 2006 (16 days). Each simulation was initialized at 1200 UTC and lasted 36 h, with 15-min time steps. The last 24 h of

every simulation is retained for further analysis. SCM time step output at the lowest model level (approximately 6-m height) is stored and is used to drive the land surface model TESSEL in separate offline simulations. Also, with this offline model the three simulations as indicated in Table 2 are performed. These offline simulations are used to evaluate the significance of the land surface–atmosphere feedbacks.

From the SCM output, diagnostics were derived that were inserted into the feedback framework [Eq. (2)]. The model does not have an a priori well-mixed temperature and specific humidity profile in the boundary layer, and also the entrainment and free atmosphere lapse rates must be aggregated from the multilayer output. The mean boundary layer temperature θ was diagnosed as the surface temperature, which is representative for the governing surface fluxes and properties. Mixing layer specific humidity q was diagnosed as the value at the lowest model level. The entrainment flux $w_e\Delta\theta$ is estimated as the minimal value of the profile of the turbulent kinematic flux of dry static energy. Boundary layer height h is taken as the height at which this minimum occurs, while $w_e\Delta q$ is the turbulent moisture flux at this height. Cubic smoothing splines are fitted through the time series data of $w_e\Delta\theta$, $w_e\Delta q$ and h to reduce the artificial step changes induced by the definition of these quantities at discrete model heights.

Effects of clouds are not explicitly included in the analysis of van Heerwaarden et al. (2010), but they do play a role in the SCM simulations by affecting the incoming radiation fluxes. The feedback with the surface energy balance, involving evaporative and nonevaporative components (Ek and Holtslag 2004), is not addressed explicitly in this study.

d. Analysis setup

Although the model simulations covered a full 7-yr period, only results for the June–August (JJA) season are used. A brief evaluation of the model skill in reproducing surface fluxes and precipitation is carried out using observations from the CESAR database. A comparison between observations and both the coupled and offline simulations is performed.

Heat wave occurrence and heat wave flux anomalies are derived from the coupled and offline simulations. The heat wave definition adopted here uses the World Meteorological Organization standard of at least 5 consecutive days with a maximum temperature of 25°C or higher, of which at least 3 days must have a maximum temperature above 30°C.

Next, the different terms in the feedback framework [Eq. (2)] are averaged for two ensembles of simulations: all JJA days and all heat wave days in JJA. Differences in forcings and feedbacks between the ensembles and between the surface types are analyzed.

Finally, the aggregated land–atmosphere feedback strength is displayed for all summer days in the 7-yr period, stratified by the incoming solar radiation and initial soil moisture content. This leads to an integrated assessment of the importance of land–atmosphere feedbacks for contrasting heat wave responses of forest and grassland.

3. Results

First, we will evaluate SCM and offline TESSEL results against observations at the Cabauw site. Next, we analyze the integrated summer energy fluxes. We investigate the mean diurnal cycle of the evapotranspiration tendency for all summer days and for the heat wave days separately. Finally, we quantify the effect of the feedbacks on the contrasting response between forest and grassland concerning the latent heat flux and atmospheric temperature.

a. Model validation

Using the actual vegetation of Cabauw (Table 2), the SCM output showed four heat waves in the period 2005–11. The three heat waves recorded in De Bilt (see previous section) were simulated well, albeit with slightly different lengths. A fourth heat wave was simulated from 7 to 15 July 2010 (9 days). For validation purposes, the flagging of heat wave episodes is taken from the SCM results. Observations of 2-m temperature, precipitation, and of the surface energy balance (SEB) terms are obtained from the CESAR database.

Averaged for all summer days (JJA) in the period 2005–11, the modeled daily mean 2-m temperature has a warm bias of 0.56 K. The root-mean-square error (rmse) is 1.18 K and the correlation between the model and observations is 0.94. Averaged over the heat wave days, the bias nearly doubles to 1.01 K and the rmse to 1.30 K. Observed mean summertime precipitation is 3.24 mm day^{-1}. This value is underestimated by the SCM by 0.38 mm day^{-1}, with an rmse of 6.25 mm day^{-1} and a correlation coefficient of 0.51. The average seasonal mean bias is approximately 17%. Considering only heat wave days, the bias is reduced to -0.28 mm day^{-1} and the rmse to 5.81 mm day^{-1}.

For both the observations and the SCM and offline models, the terms of the SEB are calculated for normal (non–heat wave) summer days. Following Teuling et al. (2010), the period 0900–1300 UTC is considered, when heating at the surface is maximal. Figure 1 shows the climatological mean SEB terms for JJA, as well as the anomalies encountered during the heat wave days.

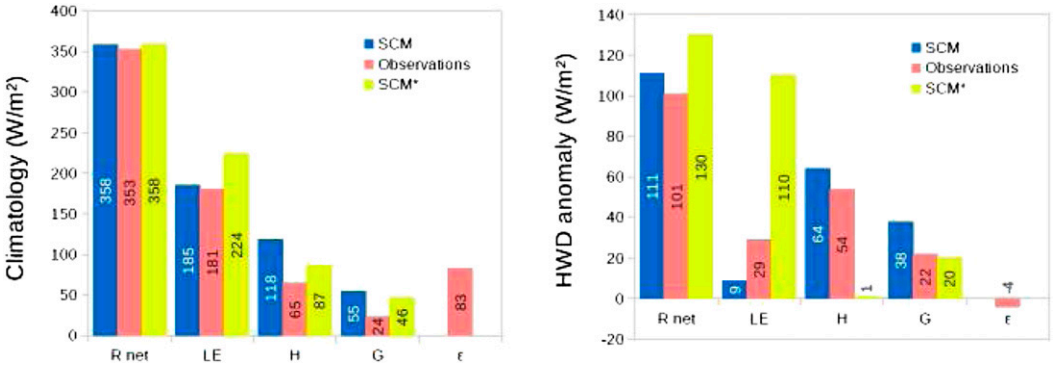

FIG. 1. (left) Summertime 0900–1300 UTC mean flux climatology over 2005–11 for net radiation, sensible heat flux, latent heat flux, and ground heat flux: SCM (blue), observations (pink), and SCM*. The term SCM* refers to SCM reruns with soil moisture held at field capacity (see text). (right) As in (left), but for anomalies during heat wave days.

On seasonal time scales, the net radiation is well captured by the model, although the modeled net radiation shows less variability (not shown). This is most likely a consequence of an underestimation of the variability of cloud occurrence. The mean model bias in net radiation is balanced by errors in cloud properties and biases in the surface temperature and associated outgoing longwave radiation.

The mean JJA latent heat flux is modeled very well by the SCM, with a positive bias of only 4 W m^{-2}. During heat wave days, the model shows hardly any evapotranspiration response, while in the observations LE is 29 W m^{-2} higher than average. The contrary is true for the sensible heat flux. The mean climatological JJA value is overestimated strongly by the SCM (118 W m^{-2}) compared to the observations (65 W m^{-2}). On heat wave days, the overestimation of sensible heat flux by the model increases to 63 W m^{-2}. This is also illustrated by the Bowen ratio H/LE shown in Table 3.

Several factors play a role here. First, the observed energy balance does not close, leading to a residual term ε. This energy balance closure problem is in accordance with the findings of Teuling et al. (2010) and is well documented in the literature [e.g., Wilson et al. (2002) for an overview and Foken et al. (2006) for the influence of land surface heterogeneity]. Second, in reality, the groundwater level at Cabauw is manually managed by the local water authorities, which generally leads to relatively shallow water tables. Groundwater processes and management are not represented in the model but can strongly influence soil moisture and thereby surface evapotranspiration (Chen and Hu 2004). An evaluation of this effect was performed by executing another set of SCM simulations, in which the initial soil water content for every daily simulation was reset to field capacity. Results are labeled by SCM* in Fig. 1 and Table 3. The climatological JJA Bowen ratio reduces to 0.39, close to the observed value of 0.36. Also during heat wave days, the Bowen ratio decreases strongly, but the correction seems to be too strong. The assumption of soil moisture at field capacity is probably not a very realistic one during the dry heat wave days.

In summary, the model captures the general dynamics of the temperature, precipitation, radiation, and turbulent fluxes fairly well. However, it is biased warm and dry, leading to too high air temperatures, too little rain and cloud formation, and an overestimation of the Bowen ratio. This bias is particularly present on heat wave days, but in general can be attributed largely to the absence of groundwater management in the simulations. As the focus of our study is the model representation of a contrasting forest and grassland response to heat waves at Cabauw, we conclude that the SCM performs well and is suitable for our purpose.

b. *Forest/grassland contrasts in the surface energy balance*

The SCM simulations for Cabauw were repeated using a surface characterization that consists of either fully grassland or full forest cover (see Table 2). The JJA 0900–1300 UTC climatology of the SEB terms is shown in Fig. 2, including the anomalies during heat wave days.

The lower albedo and lower longwave emission of forest enhances the net radiation compared to grassland.

TABLE 3. Mean Bowen ratios during all days in JJA and during the selected heat wave days.

Dataset	Mean JJA	Heat wave days
Obs	0.36	0.40
SCM	0.64	0.94
SCM*	0.39	0.26

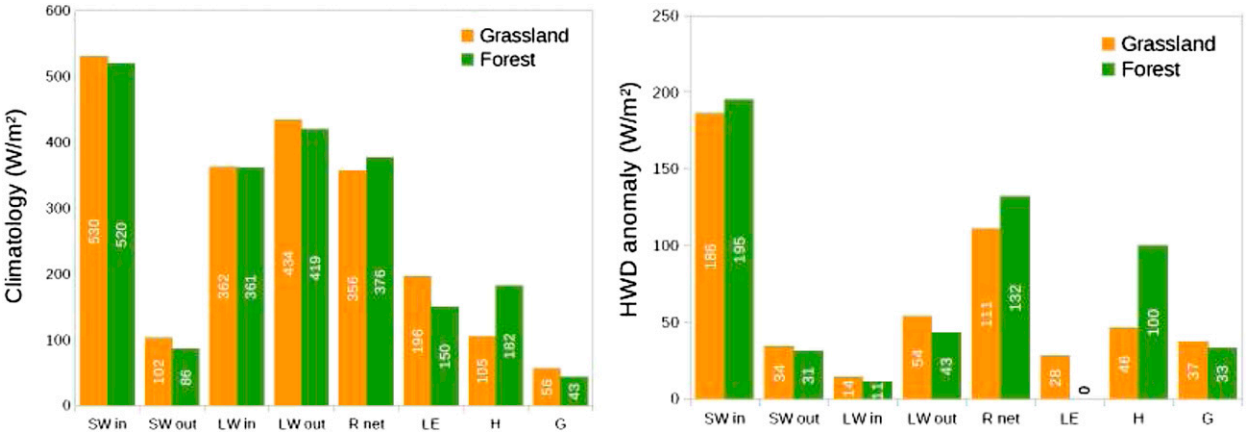

FIG. 2. (left) JJA 0900–1300 UTC mean flux climatology over 2005–11 for all SEB terms over grassland (brown) and forest (green). (right) As in (left), but for anomalies during heat wave days.

This is because surface temperature of forest is lower due to a strong coupling between surface temperature and atmospheric 2-m temperature (see also Kalma et al. 2001). Atmospheric responses to the changed surface characteristics lead to different cloud formation between the two SCM simulations, which explains the differences in incoming shortwave radiation. The extra 20 W m^{-2} net radiation received by forest is not equally distributed over the remaining energy balance terms: sensible heat flux is notably higher over forest than over grassland, while the opposite is true for latent heat flux and, to a lesser extent, the soil heat flux. During heat wave days net radiation increases stronger for forest than for grassland, and the additional energy is primarily used for sensible heat release by forest, while grassland increases its latent heat release. Compared to Teuling et al. (2010), the evapotranspiration difference between forest and grassland is more than twice as large on normal summer days (46 to their 22 W m^{-2}). The heat wave day anomaly difference, on the other hand, is smaller (28 to their 74 W m^{-2}). However, whereas we consider one site in a modest climate, Teuling et al. (2010) use an ensemble of sites with different climates and a different time period. In a qualitative sense, the results are in agreement.

c. *Diurnal cycle of evaporation*

For the purpose of comparing normal summer conditions to heat wave conditions, we have constructed normal summer day and heat wave day ensemble mean diurnal cycles for the turbulent fluxes, the atmospheric temperatures, and the terms in Eq. (2). Heat wave days are diagnosed from output from the reference SCM run. The effect of outliers is reduced by excluding the lowest and highest 12.5% of the distribution of values, leaving 27 heat wave days for analysis. Time series data are further smoothed using cubic splines to reduce the effect of clouds.

Because of a lower aerodynamic resistance for forest (not shown), the surface is coupled to the atmosphere more strongly. Under normal summer conditions this leads to a smaller difference between the temperature of the surface and of the lower atmosphere compared to grassland, leading to a lower surface temperature and a higher 2-m air temperature (both differing by about 2 K). The 2-m air temperature is the temperature 2 m above the roughness length for momentum. Because of a higher surface resistance, owing to a higher minimal surface resistance and a dependence on vapor pressure deficit, the latent heat flux is lower and, consequently, the sensible heat flux is higher in the forest case (Fig. 3, left). During heat wave day conditions, the difference between forest and grassland in all these quantities increases (Fig. 3, right): the sensible heat release and atmospheric temperature in the forest case increase more than over grassland. The latent heat flux rises strongly in the grassland case, while it remains nearly unchanged over forest. This results from a response to a number of different properties, including aerodynamic resistance and a vapor pressure deficit (VPD) dependence of surface resistance.

d. *Forcings and feedbacks*

The combined forcings derived from the latent heat tendency Eq. (2), being surface radiation forcing and boundary layer forcing, are positive but rapidly reduce throughout the morning hours, following the tendency of incident shortwave radiation (Fig. 4, left). At 1200 UTC the sun starts to descend and the forcing term changes sign, becoming increasingly negative.

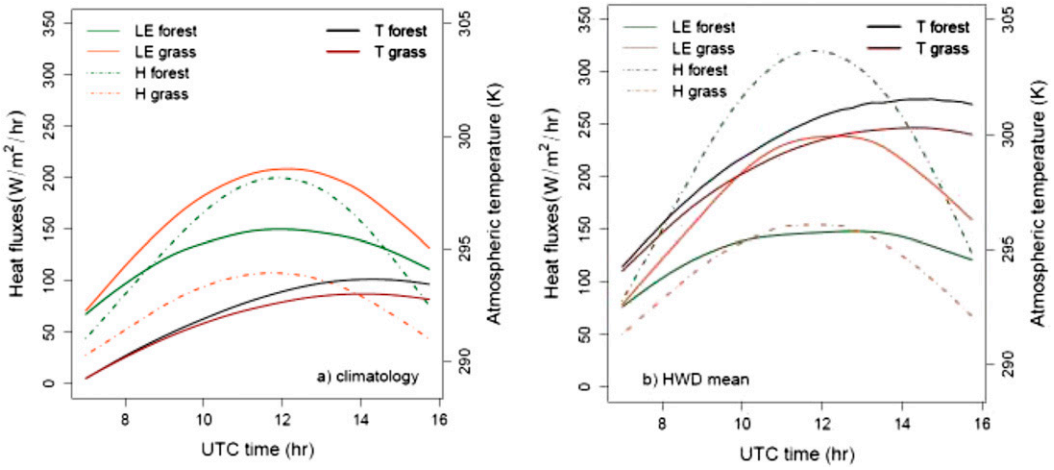

FIG. 3. Mean diurnal cycle of the (left) normal summer day and (right) heat wave day ensembles for the latent heat flux (LE), sensible heat flux (H), and 2-m air temperature (T) over forest and grass.

The effect of these forcings on the latent heat flux tendency is larger for grassland than for forest (more positive in the morning, more negative in the afternoon). This leads to a higher peak in latent heat flux and to more latent heat release integrated over the day for grass. This is mainly caused by a larger surface resistance for forest, owing to a higher minimal surface resistance and a dependence on VPD (see Table 1). In combination with a smaller aerodynamic resistance, this leads to a lower value for the amplification factor c_0 [Eq. (3)]. The VPD dependence leads to larger differences in surface resistance under heat wave conditions, as the difference between the effect of the forcings grows (Fig. 4, right).

During normal summer conditions over grassland, the combined effect of the feedbacks in Eq. (2) (boundary layer feedbacks, surface layer feedbacks, and land surface feedbacks) is to generally counteract the forcings, although during the diurnal cycle, brief episodes exist where forcings and feedbacks are of similar sign. This means that, in general, they lead to a lower latent heat flux. For a single Cabauw day studied by van Heerwaarden et al. (2010), the feedbacks tended to increase rather than decrease the forcing effects on the evaporation tendency. This different finding may be the result of the subtle balance between forcings and feedbacks encountered in this system.

For forest, the feedback is weakly positive during almost the entire daytime period, implying that evapotranspiration is increased because of feedbacks. Given the fact that, on average, evaporation over forest is smaller than over grassland, the feedbacks decrease the

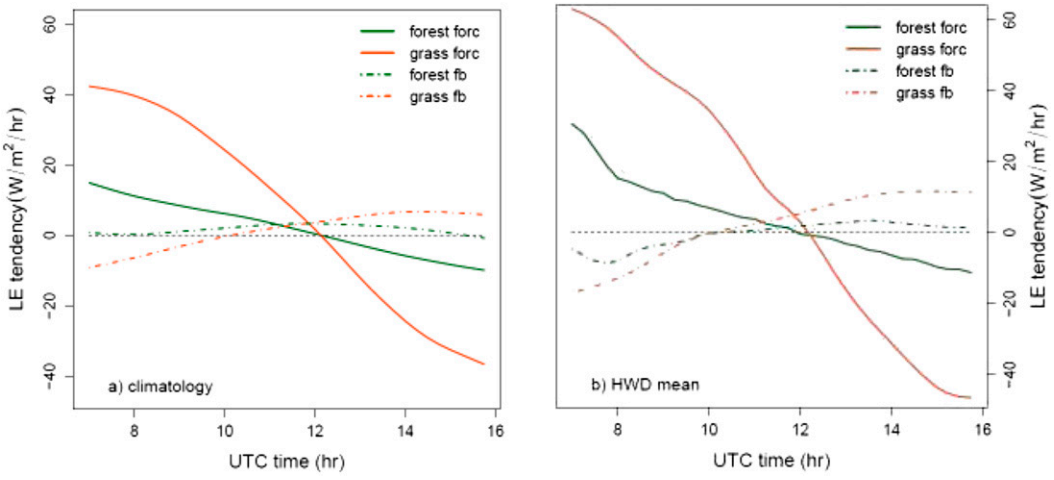

FIG. 4. As in Fig. 3, but for the combined forcing terms (forc) and the combined feedback terms (fb) in Eq. (2).

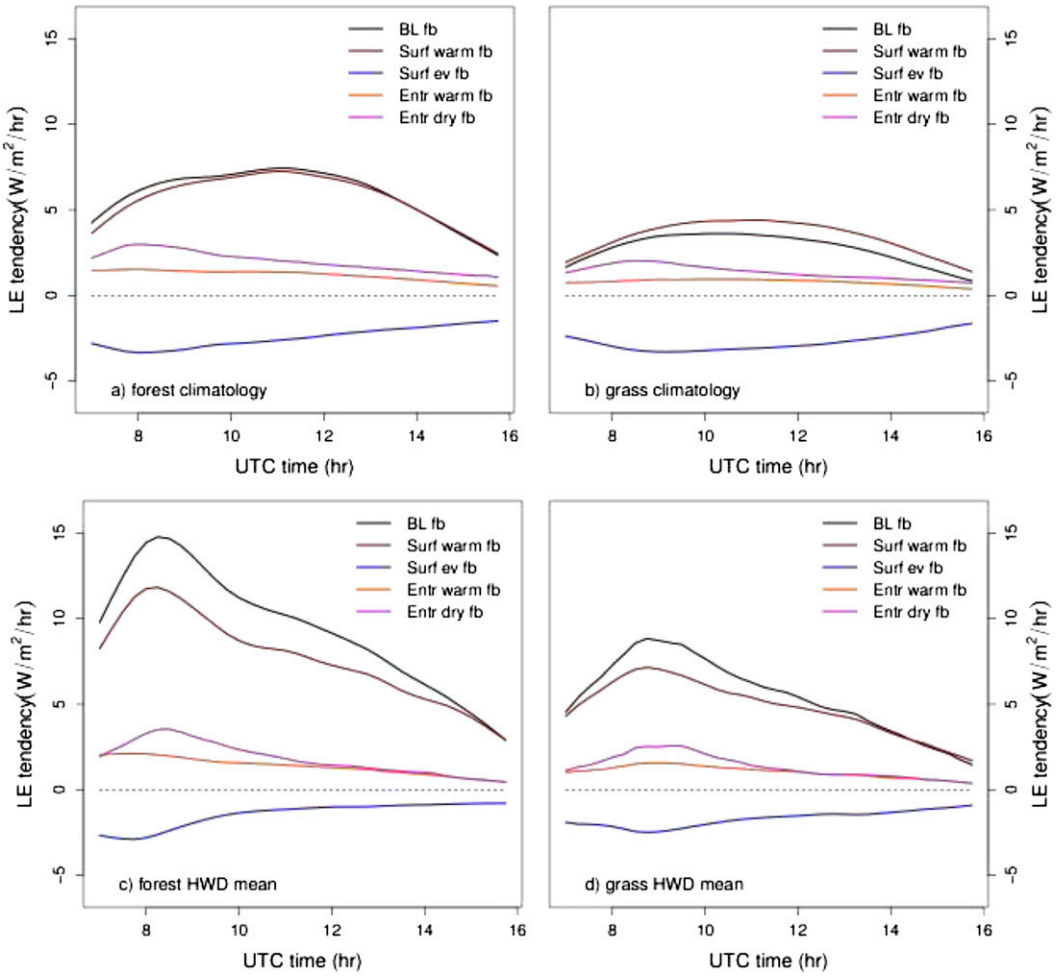

FIG. 5. Mean diurnal cycle of the (top) normal summer day and (bottom) heat wave day ensembles for the boundary layer feedbacks for (left) forest and (right) grass: Surf warm fb is surface warming feedback, Surf ev fb is surface evaporation feedback, Entr warm fb is entrainment warming feedback, Entr dry fb is entrainment drying feedback, and BL fb is net boundary layer feedbacks (sum of all these terms).

difference between latent heat release over forest and grassland during normal summer conditions.

Under heat wave conditions, the feedbacks lead to a stronger reduction of the latent heat flux in the grassland case, but in the forest case we now also see a negative feedback contribution to the latent heat flux in the morning hours. This implies that the difference between the feedback effect of grass and forest becomes slightly smaller during heat waves, so that the difference in evapotranspiration is reduced less strongly. Teuling et al. (2010) found an increased evaporation contrast during heat wave conditions, which is the combined result of contrasts in forcings and feedbacks. Our study showed qualitatively the same contrast. In the following, only the feedbacks are explored further.

We will now focus on the different feedbacks components. The net effect of the boundary layer feedbacks is positive for both forest and grassland during the whole day (Fig. 5), which implies they tend to increase latent heat release. The feedbacks are stronger (more positive) for forest than for grassland, and this difference increases during heat wave day conditions.

Forest transpires less, so the effect of the surface evaporation feedback is smaller than in the grassland case, while the surface warming feedback is relatively larger. Smaller r_a, larger H, and larger $\partial q_{\text{sat}}/\partial T$ (because of higher temperatures) are factors amplifying this surface warming feedback difference. Heat wave conditions lead to an increased surface warming feedback, because of the increased sensible heat flux. However, boundary layer growth is also increased, causing the surface warming feedback to peak earlier, when the boundary layer is not yet fully developed. While the latent heat flux is also increased in the grassland case, the surface

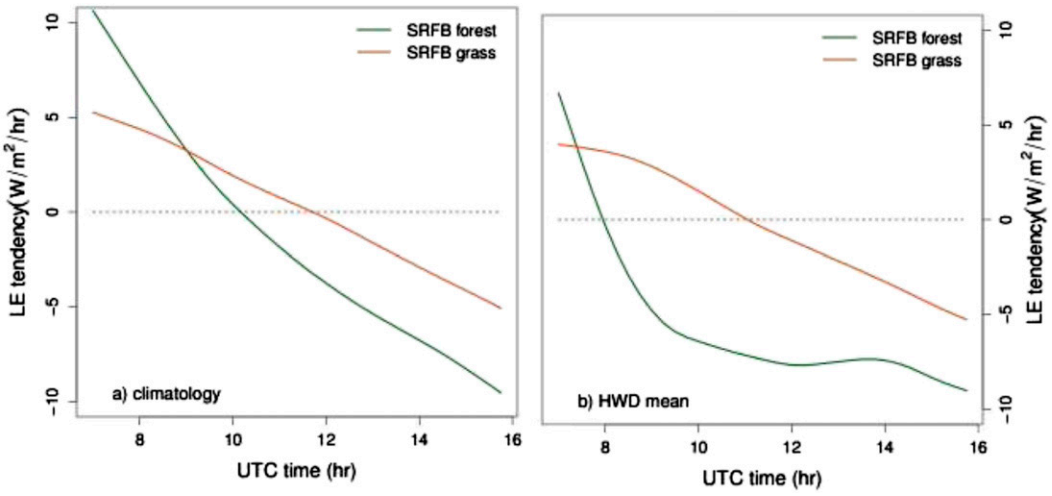

FIG. 6. Mean diurnal cycle of the (a) normal summer day and (b) heat wave day ensembles for the surface resistance feedback (SRFB).

evaporation feedback is smaller for both cases during heat waves. The increase in latent heat flux during heat waves is compensated by a smaller amplification factor c_0 (because of a higher surface resistance) and by larger boundary layer height.

Forest also entrains more warm and dry air due to increased sensible heat release. Nevertheless, the effect of the entrainment warming and entrainment drying feedback are equally large for forest and grass, as the amplification factor c_0 is smaller for forest and the boundary layer is generally higher, so that the entrained heat and moisture have to be distributed over a larger volume. The entrainment fluxes are slightly increased during heat waves in both cases, because more sensible heat release leads to more entrainment of warm and dry air. However, because of increased forcings, the feedbacks become relatively less important. Also, note that the difference between the entrainment warming and the entrainment drying feedback strength becomes smaller at higher temperatures, the entrainment warming feedback becoming relatively more important. This is accordance with the findings of van Heerwaarden et al. (2009), who found that dry air entrainment impacts more strongly at lower temperatures.

In the grassland case, the surface resistance feedback is reinforcing the forcings, acting positively on the latent heat flux in the morning and negatively in the afternoon (Fig. 6). This reflects the radiative effects on the surface resistance of the vegetation. For forest, the surface resistance starts to increase earlier in the day because of the VPD dependence. This results in the surface resistance feedback being negative for a large part of the day. Since this reduces the latent heat flux of forest, this feedback has an increasing effect on the difference in latent heat flux between forest and grassland. During heat wave days, the difference is increased even more by the feedback. For grassland, the magnitude of the surface resistance feedback during heat wave days is roughly similar to the climatological conditions, showing no sign of dry out. For forest, the VPD dependence of r_s leads to a much more negative surface resistance feedback during heat waves.

Note that the sum of the feedbacks shown in Figs. 5 and 6 does not match the results shown in Fig. 4: land surface feedbacks related to soil heat flux and longwave radiation are not negligible, but do not appear to be very different for grass and forest and are thus not shown in Fig. 6.

e. *Feedback effects*

To quantify the mean feedback contribution to the integrated latent heat release during 0900–1300 UTC, we have integrated the feedbacks over this time period twice and divided this value by the length of the integration interval, which leads to the feedback contribution to the time integrated mean latent heat flux. Since the feedback contribution is different in periods of drought and high incoming solar radiation than on normal summer days, we display the difference in feedback strength stratified by incoming solar radiation (0900–1300 UTC average, binned in 50 $\mathrm{W\,m^{-2}}$ intervals) and soil moisture content (1200 UTC value, binned in 0.01 $\mathrm{m^3\,m^{-3}}$ intervals). Forest and grassland have a different climatological evolution of soil moisture content owing to differences in evaporation. It is desirable to compare feedback contrasts for similar driving atmospheric conditions, which imprint on soil moisture anomalies. Therefore, we take a reference soil moisture value

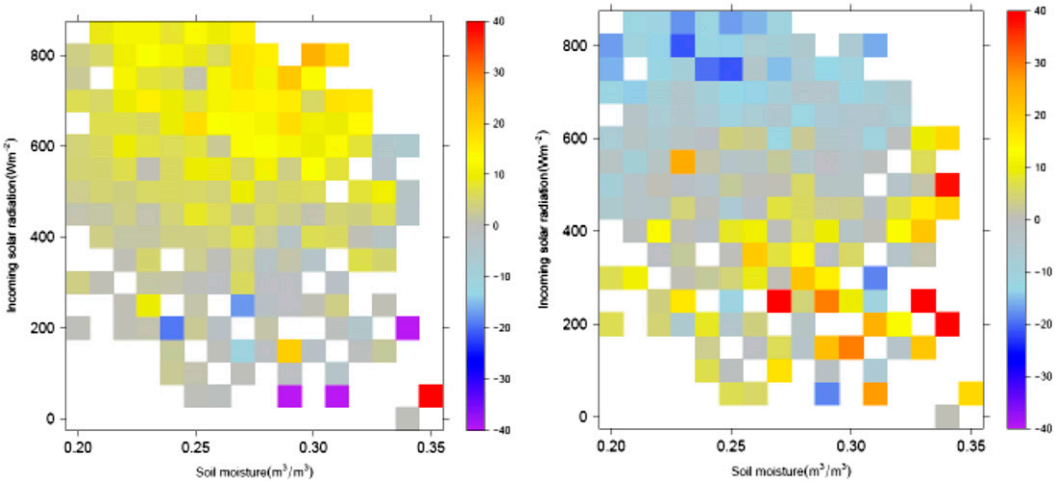

FIG. 7. Difference (W m^{-2}) between the feedback contribution to JJA 0900–1300 UTC latent heat flux [(ΔLE_{forest}) − ($\Delta LE_{grassland}$)] from forest and grassland, separating (left) the boundary layer feedbacks and (right) SRFB.

extracted from the Cabauw SCM simulation (Table 2) to stratify the soil moisture conditions of the forest and grass simulations, rather than taking the (climatologically different) simulation-specific soil moisture values. The feedbacks that show the strongest forest–grass contrasts are the boundary layer feedback and the surface resistance feedback. Their contribution to the latent heat flux is shown in Fig. 7.

In agreement with findings shown before (Fig. 5), the boundary layer feedback is generally stronger for forest than for grassland. The enhancement of the evapotranspiration is thus stronger in the forest case than for grassland, giving a negative contribution to the latent heat flux difference, since grassland generally transpires more (Fig. 7, left). On the other hand, the surface resistance feedback gives a positive contribution to this difference, being more negative for forest (Fig. 7, right). The difference between forest and grassland for both feedback types is higher for heat wave day conditions with more incoming solar radiation. However, the difference in boundary layer feedback peaks at higher soil moisture contents, when the difference in c_0 (resulting from differing r_s and surface temperature) is not too large. On the other hand, the difference in surface resistance feedback becomes maximal when the surface resistance control on total evaporation is larger, which occurs at lower soil moisture contents.

An exploration of the surface characteristics of forest and grass (Table 1) that contribute most to these boundary layer and surface resistance feedbacks was applied by rerunning the model with grassland representations of which one characteristic was copied from the forest settings: the root distribution profile, the value of $r_{s,min}$/LAI, and the factor g_d that governs the VPD dependence of r_s. From this analysis (figures not shown), it became evident that the (rather similar) specification of the root profile for forest and grassland did not lead to large effects on both feedback contributions shown in Fig. 7. The near doubling of $r_{s,min}$/LAI leads to reduced evaporation, which generally promotes the boundary layer feedback due to enhanced sensible heat release, and to a less negative (thus larger) surface resistance feedback, particularly in cases with low radiation and high soil moisture. The VPD dependence of forest is clearly the largest contributor to the negative surface resistance feedback at sunny days shown in Fig. 7b.

Together with the effect of the other feedbacks, the compensating sign of the feedbacks shown in Fig. 7 leads to a noisy difference between overall forest and grassland feedback contribution (Fig. 8). This implies that the difference in latent heat flux is not clearly enlarged or reduced because of feedbacks during heat wave days.

However, the effect of the different land–atmosphere interactions on atmospheric characteristics such as near-surface temperature and specific humidity is clearly shown in Fig. 9. As forest transpires less and releases more sensible heat, this leads to warmer and drier atmospheres. During normal summer conditions the difference is about 1 K in daily maximum 2-m air temperature and -0.5 g kg^{-1} in daily minimum near-surface specific humidity (at the lowest model level). Under conditions with more incoming solar radiation, the differences increase up to 2.5 K and -1 g kg^{-1}. This is an indication of stage I drying (Teuling et al. 2010), during which evapotranspiration is independent of soil

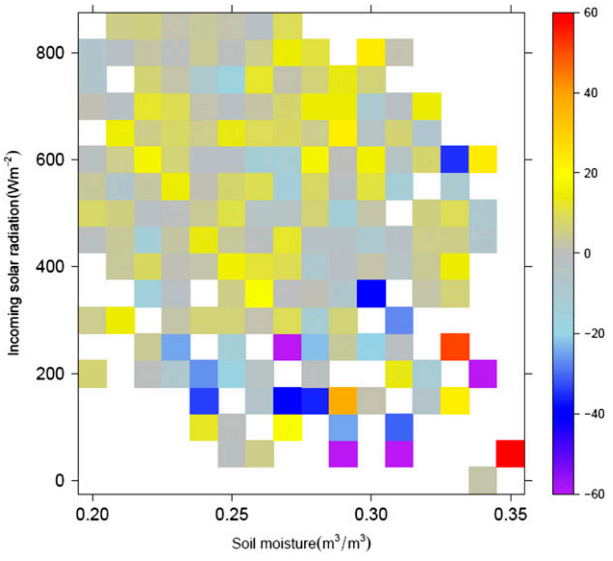

FIG. 8. As in Fig. 7, but for the total feedback contribution to LE differences.

moisture. For very low soil moisture content the differences decrease, because grassland starts to dry out and transpiration is limited. This is evident by a higher value of the water stress function in the grassland case of up to 250% of the forest case (not shown). Since evapotranspiration is still larger in the grassland case, the stage II drying reported by Teuling et al. (2010) is not yet reached. This is a consequence of the investigated site, Cabauw, which has a mild Dutch climate with a limited number of long-lasting dry conditions necessary for stage II drying. In drier midlatitude regions, larger effects of soil depletion can be expected. The strength of this effect is also determined by the difference in root profile between the vegetation types.

A direct illustration of the importance of land–atmosphere feedbacks is a comparison of the forest/grassland evaporation contrast calculated with the SCM (allowing for land–atmosphere feedbacks) and with the offline land model TESSEL (where atmospheric properties are prescribed). Multiple TESSEL simulations were carried out, forced by each of the surface characterizations represented in the SCM (see Table 2). Figure 10 shows the forest–grass contrast for the SCM simulations and for two sets of TESSEL simulations driven by atmospheric conditions from the forest and grass SCM configurations (see Fig. 9).

Somewhat surprisingly, the different atmospheric conditions do not lead to systematic differences in the grass–forest contrast generated by the offline TESSEL simulations (Fig. 10, bottom). For the drier and warmer atmospheric conditions generated by the forest SCM configuration, LE calculated by TESSEL is higher for both forest and grassland (not shown), but the contrast is not affected. Apparently, the higher evaporation rates do not lead to strong soil moisture depletion or a dry-down regime for the grassland representation in TESSEL.

The forest–grass contrast calculated by the SCM is generally of smaller amplitude than that calculated by TESSEL, particularly during heat wave conditions, when the atmospheres of grassland and forest differ strongly in the SCM (Fig. 11). This implies that the land–atmosphere feedbacks do reduce the forest/grass contrast, which is consistent with the generally negative sign of the feedbacks involved (see section 2). Offline simulations with different land surface types thus tend to overestimate the magnitude of this contrast by about 10% on normal summer days to 30% during heat waves.

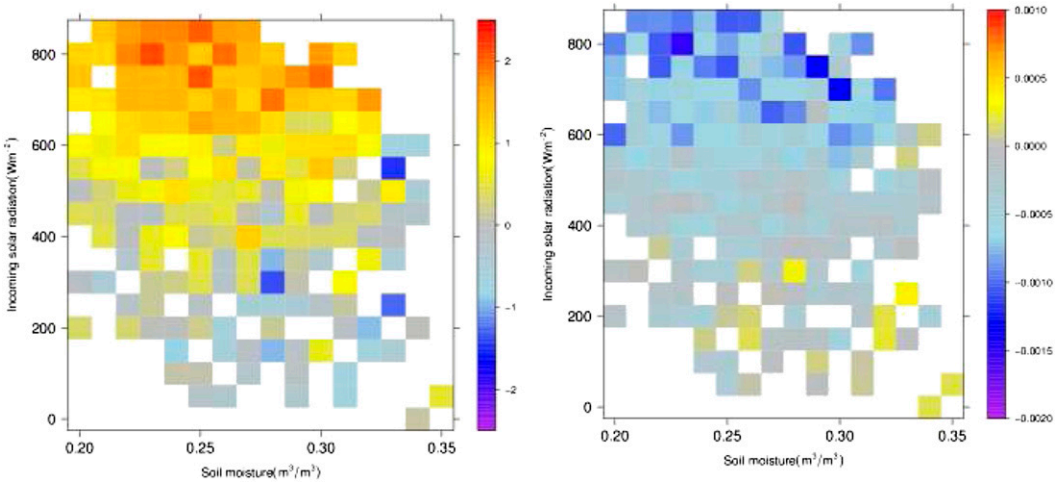

FIG. 9. Difference between forest and grassland in the summer daily (left) maximum 2-m air temperature and (right) minimum near-surface specific humidity.

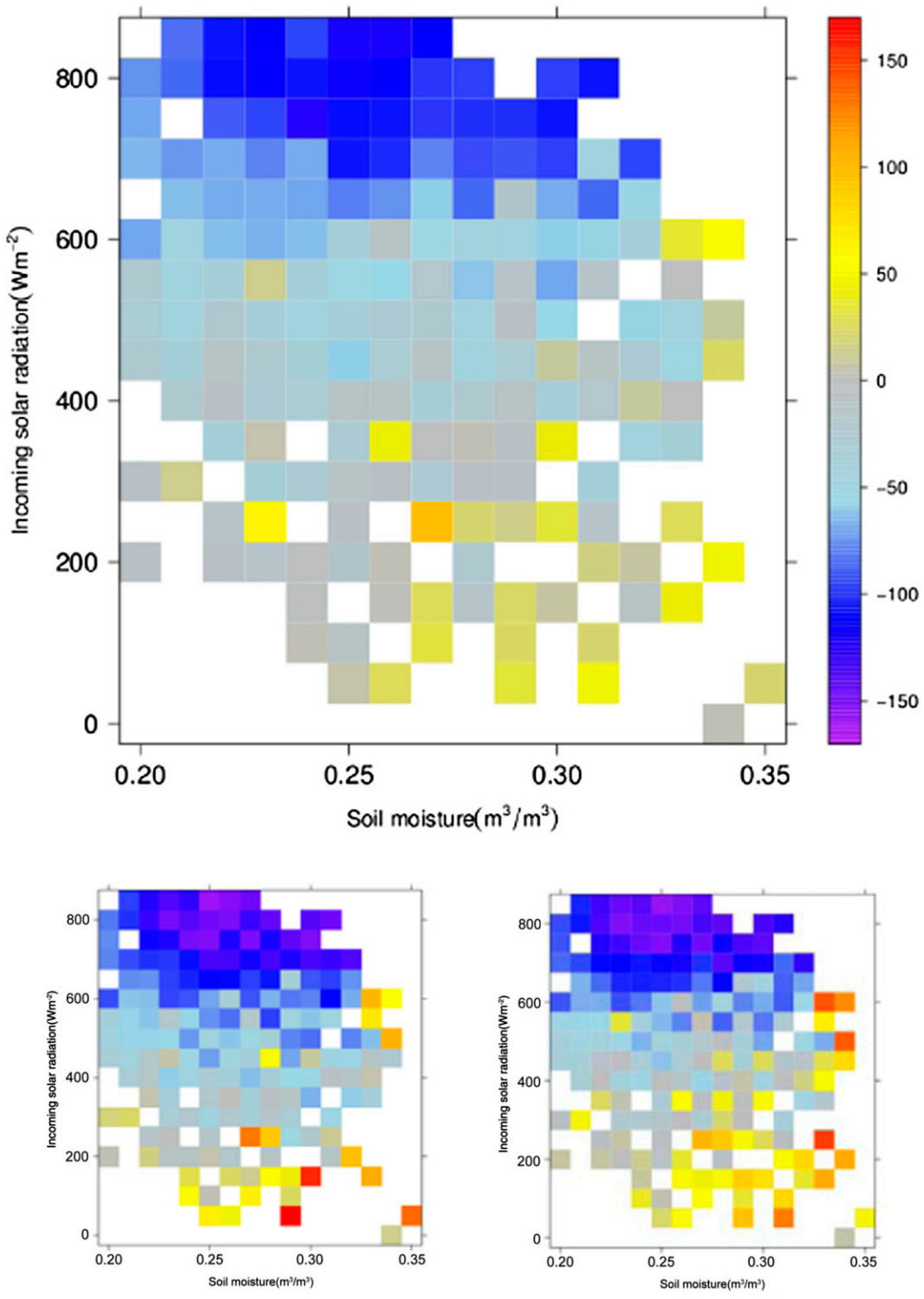

FIG. 10. Difference between forest and grassland in summer 0900–1300 UTC mean latent heat flux calculated (top) by the SCM; and by TESSEL driven by the SCM (bottom left) grassland and (bottom right) forest runs.

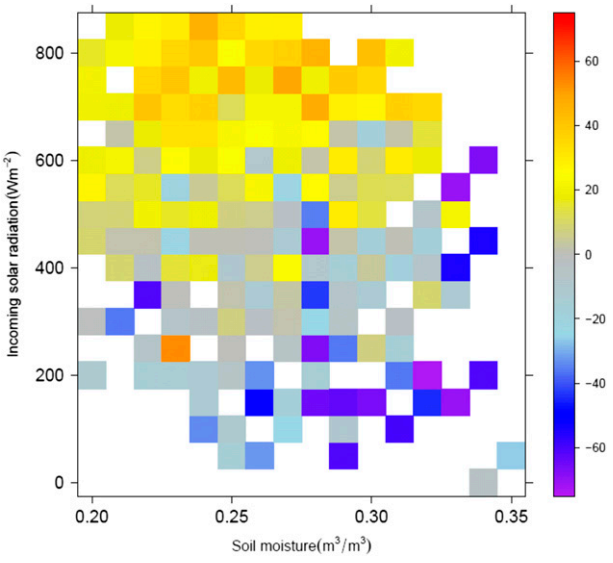

FIG. 11. Difference between forest and grassland 0900–1300 UTC mean summer latent heat flux, calculated by RACMO SCM (Fig. 10, top) minus that calculated by TESSEL, with forcing from the grassland case (Fig. 10, bottom left).

4. Summary and conclusions

To assess the importance of land–atmosphere feedbacks in the difference between the response of forest and grassland surface energy fluxes to heat waves, simulations with a single-column model (SCM) have been carried out. The setup of the SCM represented Cabauw (the Netherlands) for a 7-yr period (2005–11), while different land surface conditions were employed (a reference run with the actual vegetation cover and two runs with either full forest or full grassland cover). The energy balance of the reference run showed good agreement with observations when the effect of artificial groundwater management on surface evaporation was represented (in some form).

The surface evaporation tendency framework developed by van Heerwaarden et al. (2010) is used to determine the effects of the land–atmosphere feedbacks on the latent heat flux for forest and grassland. Normal summer days were distinguished from heat wave days, as diagnosed from the modeled 2-m temperature time series. Next, the feedback contribution to the 0900–1300 UTC latent heat flux was evaluated after stratification by incoming solar radiation and soil moisture content of the reference run. In addition, the forest–grass contrast in average latent heat flux in the SCM runs was compared to the differences obtained with offline TESSEL simulations with atmospheric boundary conditions obtained by the SCM runs.

The SCM results reproduce the observation-based findings of Teuling et al. (2010) qualitatively: the difference in Bowen ratio between forest and grassland increases during heat wave conditions, as forests spend most of the excess energy received during heat waves on sensible heat release, while grasslands increase the latent heat release. This difference is mainly the result of a difference in the VPD forcing. While both vegetation types receive nearly similar amounts of radiation, the VPD increases during heat waves, resulting in a larger surface resistance for forest and a weaker response to the effect of incoming radiation.

In contrast, Findell et al. (2007) found that the decreased rooting depth is the main factor determining the difference between grassland and forest in the same study area. Although they used another type of forest (broadleaf deciduous), which has a larger rooting depth both in their model and ours, this shows that the results are dependent on model parameters of the soil as well.

Boundary layer feedbacks and surface resistance feedbacks are quite different for forest and grassland, but tend to compensate each other in terms of modifying the surface evaporation contrast. The effect of the boundary layer feedbacks is to decrease the difference between forest and grassland latent heat flux, as the increased sensible heat release in the forest case will lead to a warmer and drier atmosphere and consequently higher evaporation rates. On the other hand, the surface resistance feedback increases the latent heat flux difference between forest and grassland because the increasing VPD during the day increases the surface resistance of forest, which has a negative impact on evapotranspiration. Different representations of the surface type–specific responses and feedbacks in current weather and climate model may partly explain the currently observed lack of agreement in responses to land use change as reported by, for instance, Pitman et al. (2012).

We particularly see the effect of stage I drying (Teuling et al. 2010) and only a small step toward stage II drying. Cabauw has a mild climate and does not very often experience severe droughts. Results are expected to be different in areas where soil moisture is regularly depleted. A study of a drier region, where soil moisture limitation particularly of the upper soil layers becomes dominant and stage II—III drying is reached, is an important subject for further research.

Although the feedbacks do not lead to a strong forest–grass evaporation contrast, the atmosphere of forest is generally drier and warmer during conditions of elevated incoming radiation. The fact that the coupling with the atmosphere is important is illustrated by comparing the SCM runs with offline runs from the uncoupled land surface model (TESSEL), with both land surface characterizations forced with the same atmosphere (forest or grass). Although the choice of the atmospheric

forcing does not affect the forest–grass contrast in the TESSEL runs significantly, these contrasts are larger than in the SCM simulations where feedbacks are allowed, particularly during heat wave conditions. This implies that forest–grass contrasts in response to heat waves using offline land models will be overestimated when a single forcing time series is used for both surface types. Figure 11 gives a flavor of this overestimation in terms of surface evaporation, specific for the conditions encountered in the Cabauw climate regime. It also suggests that evaluation of land use change on regional climatological conditions like heat wave resilience cannot be adequately performed with offline model simulations alone.

Our conceptualization of ''forest'' and ''grass'' is very simplistic and strongly refers to the philosophy with which these surface types are represented in models. In reality, the stomatal response to dry and/or warm conditions is governed by complex physical, biological, and chemical processes, which are only conceptually represented in the models and (Dutch) climate conditions explored here. Also, the notion of ''forest'' and ''grass'' does not give justice to the many different species and ecosystems that have developed a wide range of drought strategies. A more biophysical modeling approach, including new modeling concepts of drought strategies (van der Molen et al. 2011), is definitely justified. Similarly, modeling concepts of soil hydraulics and evaporation regimes characterized by soil moisture limitation (Teuling et al. 2009) must be explored further in the future.

Acknowledgments. Discussions with Ryan Tueling, technical assistance by Peter Baas and Bert van Ulft, and a review of an early version of this manuscript by Fred Bosveld are highly appreciated. Three anonymous reviewers are thanked for their comments, which have helped to improve the quality of the paper.

REFERENCES

Chen, X., and Q. Hu, 2004: Groundwater influences on soil moisture and surface evaporation. *J. Hydrol.,* **297,** 285–300, doi:10.1016/j.jhydrol.2004.04.019.

Ciais, Ph., and Coauthors, 2005: Europe-wide reduction in primary productivity caused by the heat and drought in 2003. *Nature,* **437,** 529–533, doi:10.1038/nature03972.

Dole, R., and Coauthors, 2011: Was there a basis for anticipating the 2010 Russian heat wave? *Geophys. Res. Lett.,* **38,** L06702, doi:10.1029/2010GL046582.

Ek, M. B., and A. A. M. Holtslag, 2004: Influence of soil moisture on boundary layer cloud development. *J. Hydrometeor.,* **5,** 86–99, doi:10.1175/1525-7541(2004)005<0086:IOSMOB>2.0.CO;2.

Findell, K. L., E. Shevliakova, P. C. D. Milly, and R. J. Stouffer, 2007: Modeled impact of anthropogenic land cover change on climate. *J. Climate,* **20,** 3621–3634, doi:10.1175/JCLI4185.1.

——, P. Gentine, B. R. Lintner, and C. Kerr, 2011: Probability of afternoon precipitation in eastern United States and Mexico enhanced by high evaporation. *Nat. Geosci.,* **4,** 434–439, doi:10.1038/ngeo1174.

Fischer, E. M., S. I. Seneviratne, D. Luthi, and C. Schär, 2007: Contribution of land-atmosphere feedbacks to recent European summer heat waves. *Geophys. Res. Lett.,* **34,** L06707, doi:10.1029/2006GL029068.

Foken, T., F. Wimmer, M. Mauder, C. Thomas, and C. Liebethal, 2006: Some aspects of the energy balance closure problem. *Atmos. Chem. Phys.,* **6,** 4395–4402, doi:10.5194/acp-6-4395-2006.

Hazeleger, W., and Coauthors, 2012: EC-Earth V2.2: Description and validation of a new seamless Earth system prediction model. *Climate Dyn.,* **39,** 2611–2629, doi:10.1007/s00382-011-1228-5.

Hirschi, M., and Coauthors, 2011: Observational evidence for soil-moisture impact on hot extremes in southeastern Europe. *Nat. Geosci.,* **4,** 17–21, doi:10.1038/ngeo1032.

Jacobs, C. M. J., and H. A. R. De Bruin, 1992: The sensitivity of regional transpiration to land-surface characteristics: Significance of feedback. *J. Climate,* **5,** 683–698, doi:10.1175/1520-0442(1992)005<0683:TSORTT>2.0.CO;2.

Kalma, J. D., S. W. Franks, and B. J. J. M. van den Hurk, 2001: On the representation of land surface fluxes for atmospheric modelling. *Meteor. Atmos. Phys.,* **76,** 53–76, doi:10.1007/s007030170039.

Neggers, R. A. J., 2009: A dual mass flux framework for boundary layer convection. Part II: Clouds. *J. Atmos. Sci.,* **66,** 1489–1506, doi:10.1175/2008JAS2636.1.

——, M. Koehler, and A. A. M. Beljaars, 2009: A dual mass flux framework for boundary-layer convection. Part I: Transport. *J. Atmos. Sci.,* **66,** 1465–1487, doi:10.1175/2008JAS2635.1.

——, A. P. Siebesma, and T. Heus, 2012: Continuous single-column model evaluation at a permanent meteorological supersite. *Bull. Amer. Meteor. Soc.,* **93,** 1389–1400, doi:10.1175/BAMS-D-11-00162.1.

Pitman, A. J., and Coauthors, 2012: Effects of land cover change on temperature and rainfall extremes in multi-model ensemble simulations. *Earth Syst. Dyn.,* **3,** 213–231, doi:10.5194/esd-3-213-2012.

Seneviratne, S. I., T. Corti, E. L. Davin, M. Hirschi, E. B. Jaeger, I. Lehner, B. Orlowsky, and A. J. Teuling, 2010: Investigating soil moisture–climate interactions in a changing climate: A review. *Earth Sci. Rev.,* **99,** 125–161, doi:10.1016/j.earscirev.2010.02.004.

Sheffield, J., E. F. Wood, and M. Roderick, 2012: Little change in global drought over the past 60 years. *Nature,* **491,** 435–438, doi:10.1038/nature11575.

Taylor, C. M., R. A. M. de Jeu, F. Guichard, P. P. Harris, and W. A. Dorigo, 2012: Afternoon rain more likely over drier soils. *Nature,* **489,** 423–426, doi:10.1038/nature11377.

Tennekes, H., 1973: A model for the dynamics of the inversion above a convective boundary layer. *J. Atmos. Sci.,* **30,** 558–567, doi:10.1175/1520-0469(1973)030<0558:AMFTDO>2.0.CO;2.

Teuling, A. J., and Coauthors, 2009: A regional perspective on trends in continental evaporation. *Geophys. Res. Lett.,* **36,** L02404, doi:10.1029/2008GL036584.

——, and Coauthors, 2010: Contrasting response of European forest and grassland energy exchange to heatwaves. *Nat. Geosci.,* **3,** 722–727, doi:10.1038/ngeo950.

van den Hurk, B. J. J. M., P. Viterbo, A. C. M. Beljaars, and A. K. Betts, 2000: Offline validation of the ERA40 surface scheme. ECMWF Tech. Memo. 295, 42 pp.

——, M. Best, P. Dirmeyer, A. Pitman, J. Polcher, and J. Santanello, 2011: Acceleration of land surface model development over a decade of glass. *Bull. Amer. Meteor. Soc.,* **92,** 1593–1600.

van der Molen, M. K., and Coauthors, 2011: Drought and ecosystem carbon cycling. *Agric. For. Meteor.,* **151,** 765–773, doi:10.1016/j.agrformet.2011.01.018.

van Heerwaarden, C. C., J. Vila-Guerau de Arellano, A. F. Moene, and A. A. M. Holtslag, 2009: Interactions between dry-air entrainment, surface evaporation and convective boundary layer development. *Quart. J. Roy. Meteor. Soc.,* **135,** 1277–1291, doi:10.1002/qj.431.

——, ——, A. Gounou, F. Guichard, and F. Couvreux, 2010: Understanding the daily cycle of evapotranspiration: A method to quantify the influence of forcings and feedbacks. *J. Hydrometeor.,* **11,** 1405–1422, doi:10.1175/2010JHM1272.1.

van Meijgaard, E., L. H. van Ulft, W. J. van de Berg, F. C. Bosveld, B. J. J. M. van den Hurk, G. Lenderink, and A. P. Siebesma, 2008: The KNMI regional atmospheric climate model RACMO version 2.1. KNMI TR 302, 43 pp. [Available online at http://a.knmi2.nl/knmi-library/knmipubTR/TR302.pdf.]

van Ulden, A. P., and J. Wieringa, 1996: Atmospheric boundary layer research at Cabauw. *Bound.-Layer Meteor.,* **78,** 39–69, doi:10.1007/BF00122486.

Wilson, K., and Coauthors, 2002: Energy balance closure at FLUXNET sites. *Agric. For. Meteor.,* **113,** 223–243, doi:10.1016/S0168-1923(02)00109-0.

Zaitchik, B. F., A. K. Macalady, L. R. Bonneau, and R. B. Smith, 2006: Europe's 2003 heat wave: A satellite view of impacts and land–atmosphere feedbacks. *Int. J. Climatol.,* **26,** 743–769, doi:10.1002/joc.1280.

Zeng, X., Y.-J. Dai, R. E. Dickinson, and M. Shaik, 1998: The role of root distribution for climate simulation over land. *Geophys. Res. Lett.,* **25,** 4533–4536, doi:10.1029/1998GL900216.